Research Square

Preprints are preliminary reports that have not undergone peer review.
They should not be considered conclusive, used to inform clinical practice,
or referenced by the media as validated information.

Global sensitivity and identifiability of Structured Cam Clay parameters for cement-treated clays: a variance-based analysis with a staged calibration protocol

Alhassan Ahmed Igbeneghu

alhassanahmedi@auchipoly.edu.ng

University of Benin

Ngozi Kayode-Ojo

University of Benin

Samuel Adesina Adegbemileke

University of Benin

Research Article

Keywords: Structured Cam Clay, Cement-treated clay, Global sensitivity analysis, Sobol' indices, Parameter identifiability, Critical state, Constitutive model calibration

Posted Date: November 16th, 2026

DOI: https://doi.org/10.21203/rs.3.rs-11595166/v1

License: This work is licensed under a Creative Commons Attribution 4.0 International License.
Read Full License

Additional Declarations: No competing interests reported.

Global sensitivity and identifiability of Structured Cam Clay parameters for cement-treated clays: a variance-based analysis with a staged calibration protocol

Article type: Research

Alhassan Ahmed Igbeneghu[1*], **Ngozi Kayode-Ojo**[2], **Samuel Adesina Adegbemileke**[3]

[1] Department of Civil Engineering, University of Benin, Benin City, Edo State, Nigeria

[2] Department of Civil Engineering, Auchi Polytechnic, Auchi, Edo State, Nigeria

*Corresponding author: Alhassan Ahmed Igbeneghu, alhassanahmedi@auchipoly.edu.ng

E-mail addresses: Alhassan Ahmed Igbeneghu, alhassanahmedi@auchipoly.edu.ng; Ngozi Kayode-Ojo, ngozi.kayode-ojo@uniben.edu; Samuel Adesina Adegbemileke, samuel.adegbemileke@uniben.edu

Abstract

The Structured Cam Clay (SCC) model is attractive for cement-treated clays because it adds only a few parameters to Modified Cam Clay. However, how those parameters control the predicted response, and whether they can be recovered from routine laboratory tests, has so far been examined only one parameter at a time. This study reports a variance-based global sensitivity and identifiability analysis of SCC extended for cohesion. A vectorised strain-driven integrator was written for conventional drained and undrained triaxial compression and verified against closed-form Modified Cam Clay solutions to within 0.12%. Seven parameters were sampled over ranges representative of lightly to moderately cemented clays, and first-order and total-order Sobol′ indices were computed from 18 432 simulations per stress path.

Undrained peak strength depended almost entirely on cohesion and the critical state stress ratio (total-order indices 0.73 and 0.26), while the compressibility and structure parameters governed only the strain needed to reach it. Under drained loading, the additional void ratio and the destructuring index dominated volume change and stiffness (total-order indices 0.68 and 0.71). Whenever structure was significant, the undrained strength reduced to a simple closed form, $q_{max} \approx (M^{*}p'_{y,i} + C)/2$, which was accurate to within 5% for 92% of the sampled parameter sets and is a lower bound to the full solution. A rejection-sampling analysis of 200 000 parameter sets showed that the critical state stress ratio and cohesion trade off almost perfectly in a single undrained test, and that the swelling index cannot be identified from triaxial stress–strain curves even when drained and undrained tests are combined. On this basis, a staged calibration protocol is proposed in which each parameter is fixed from the measurement that isolates it, and the protocol is applied to five cement-treated sandy clays from Southwest Nigeria. The results show that parameter influence is a property of the parameter, the output and the stress path together, and that a soil unremarkable in undrained strength can be the most compressible in drained shear.

Keywords: Structured Cam Clay; Cement-treated clay; Global sensitivity analysis; Sobol′ indices; Parameter identifiability; Critical state; Constitutive model calibration

Introduction

Cement mixing is now a routine remedy for soft clay beneath embankments, pavements and light structures, from the marine clays of South-East Asia to the lagoonal deposits of the West African coast. The hydration products bond the particles and give the soil a structure it did not previously have. That structure raises strength and lowers compressibility, but it also degrades under load [1-4]. Strength development has been related to the clay-water/cement ratio and to the microstructure of the hydration products [5, 6], and the post-yield behaviour of cemented

clays has been interpreted within critical state frameworks extended for bonding [7, 8]. The general effects of structure on compressibility and strength, first systematised for natural clays [9-11], apply with even greater force to artificially cemented soils.

Constitutive models for these materials must therefore represent both the bonded state and its loss. Several do so with considerable sophistication, coupling cementation, destructuring and fabric anisotropy [12-18]. Each additional mechanism, however, brings parameters that must be calibrated from tests that practitioners may not have. The Structured Cam Clay (SCC) model of Liu and Carter [19] sits at the economical end of this spectrum. It retains the Modified Cam Clay (MCC) framework [20-22] and adds a structural void ratio that decays with stress, a destructuring index and a flow-rule parameter. Later versions represent cementation through a cohesion term that shifts the yield surface into tension [23-25]. The model has been calibrated for cemented Bangkok, Ariake and other clays with good results, and its compact parameter set makes it a natural candidate for routine design.

Two questions nonetheless remain open. The first is which parameters actually control the predicted response, and whether that ranking depends on the stress path. Published parametric studies of SCC, including a recent comparative study of cement-treated soils [26], vary one parameter at a time about a single reference set. Such local analyses cannot detect interactions, and their results depend on the reference point [27, 28]. Variance-based global methods, built on the decomposition of Sobol′ [29, 30], overcome both limitations and have become standard in other branches of engineering modelling, but they have rarely been applied to critical state models of structured soils. The second question is whether the parameters can be recovered from the tests usually available. A model may reproduce a stress-strain curve with many different parameter combinations, and in that case the calibrated values have no physical meaning [31, 32]. In geotechnics, this problem has been recognised in

back-analysis and inverse modelling [33–35] and in optimisation-based calibration of soil models [36, 37], but it has not been examined systematically for SCC.

This study addresses both questions for SCC with cohesion under conventional drained and undrained triaxial compression. Its objectives were to: (i) implement and verify a strain-driven integration of the model for both stress paths; (ii) quantify the influence of seven parameters on strength, stiffness, pore pressure and volume change with variance-based (Sobol′) indices; (iii) explain the dominant sensitivities mechanically and, where possible, in closed form; (iv) assess which parameters can be identified from undrained, drained or combined test data; and (v) turn the results into a calibration protocol and apply it to five cement-treated sandy clays. The contributions are a stress-path-dependent ranking of SCC parameters with quantified uncertainty, a closed-form lower bound for the undrained strength of structured cemented clay, evidence of a near-perfect trade-off between the critical state stress ratio and cohesion, and a staged calibration procedure that avoids that trade-off. The overall approach is summarised in Fig. 1.

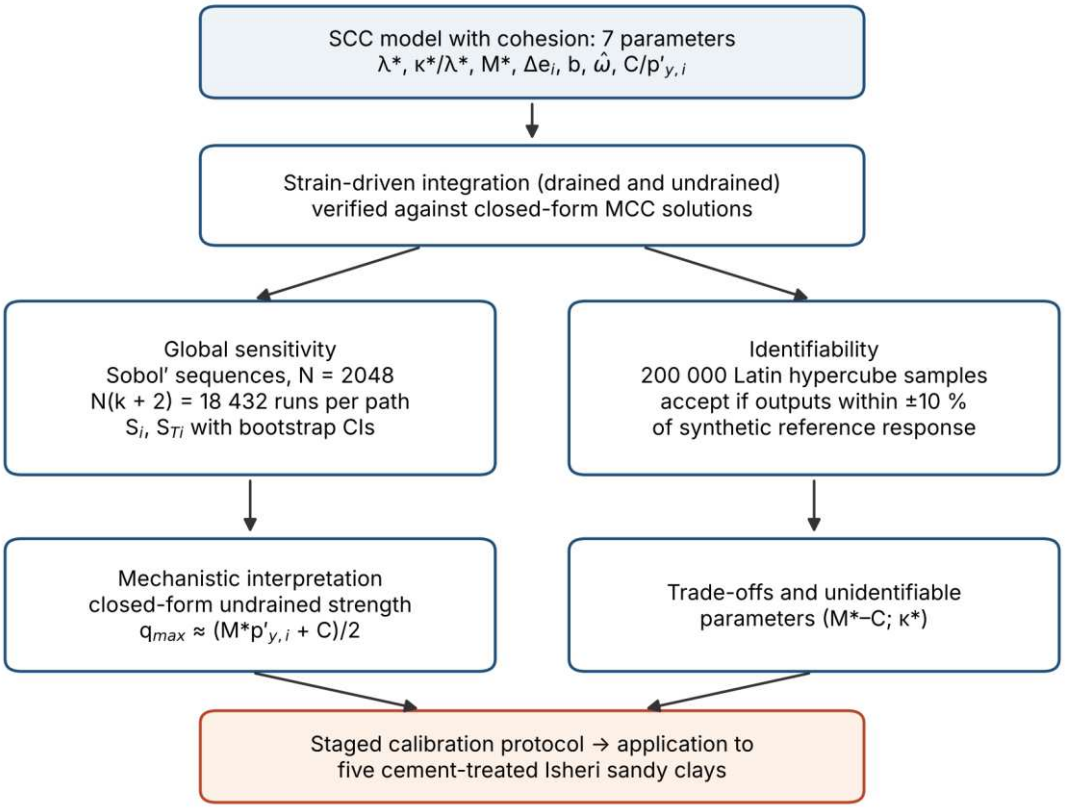


Fig. 1 Workflow of the study, from model implementation and verification to global sensitivity, identifiability and the staged calibration protocol

Methods

Structured Cam Clay model with cohesion

The model is summarised here in triaxial stress space (p′, q) for completeness; full derivations are given by Liu and Carter [19] and Horpibulsuk et al. [23]. A list of symbols is given in the Nomenclature at the end of the paper. During virgin yielding, the void ratio of the structured soil, e, exceeds that of the reconstituted soil, e*, by an additional void ratio Δe that decays as the size of the structural yield surface, p′$_s$, grows:

$$e = e^* + \Delta e, \qquad \Delta e = \Delta e_i \left(\frac{p'_{y,i}}{p'_s} \right)^b \qquad (1)$$

$$e^* = e^*_{IC} - \lambda^* \ln p' \qquad (2)$$

where λ* is the intrinsic compression index, Δe_i is the additional void ratio at first virgin yield, $p'_{y,i}$ is the mean effective stress at first virgin yield and b is the destructuring index. Cementation is introduced by shifting the mean effective stress by C/M* [23], so that the yield surface is

$$f = q^2 - M^{*2}\,\bar{p}'(\bar{p}'_s - \bar{p}') = 0, \qquad \bar{p}' = p' + \frac{C}{M^*} \qquad (3)$$

with $\bar{p}'_s = p'_s + C/M^*$. The peak strength line is therefore $q = M^* p' + C$. The plastic volumetric strain contains an intrinsic part and a structural part that grows without limit as the stress ratio $\bar{\eta} = q/\bar{p}'$ approaches M*:

$$d\varepsilon_v^p = \left[(\lambda^* - \kappa^*) + b\,\Delta e\,\frac{M^*}{M^* - \bar{\eta}}\right]\frac{dp'_s}{(1+e)\,p'_s} \equiv A\,\frac{dp'_s}{(1+e)\,p'_s} \qquad (4)$$

Structure also reduces the ratio of plastic deviatoric to plastic volumetric strain through the flow-rule parameter ω, subject to $0 \le \omega \le 1/\Delta e_i$:

$$\frac{d\varepsilon_d^p}{d\varepsilon_v^p} = D(\bar{\eta}) = \frac{2\,(1 - \omega\,\Delta e)\,\bar{\eta}}{M^{*2} - \bar{\eta}^2} \qquad (5)$$

Elastic strains follow from the swelling index κ* and a constant Poisson's ratio ν:

$$K = \frac{(1+e)\,p'}{\kappa^*} \qquad (6)$$

$$G = \frac{3\,(1-2\nu)}{2\,(1+\nu)}\,K \qquad (7)$$

In the full model, cohesion degrades with plastic strain. It is held constant here, which isolates its effect on peak strength and matches the scope of most published calibrations of cemented clays at small to moderate strain.

Numerical implementation

Conventional triaxial compression was simulated from an isotropic state on the virgin yield surface, $p'_0 = p'_{s0} = p'_{y,i} = 100$ kPa, to a deviatoric strain of 20%. Each increment of deviatoric strain $d\varepsilon_d$ was split into elastic and plastic parts, with plastic multiplier $\Lambda = d\varepsilon_v^p$ and $d\varepsilon_d^p = \Lambda D(\bar{\eta})$. Writing $f_p = \partial f/\partial p'$, $f_q = \partial f/\partial q$ and $H = (\partial f/\partial p'_s)(1 + e)p'_s/A$, the consistency condition gives, for undrained loading ($d\varepsilon_v = 0$),

$$\Lambda = \frac{3G\, f_q\, d\varepsilon_d}{K f_p + 3G\, f_q\, D(\bar{\eta}) - H} \qquad (8)$$

and, for drained loading at constant cell pressure ($dq = 3dp'$),

$$\Lambda = \frac{G\, d\varepsilon_d}{G\, D(\bar{\eta}) - \dfrac{H}{f_p + 3f_q}} \qquad (9)$$

The stresses were then updated elastically, p'_s was updated from Eq. (4), and the void ratio from the volumetric strain. After each increment, p'_s was adjusted so that the stress point lay exactly on the yield surface. This consistent drift correction [38] removed accumulated departure from the yield surface without the explicit error-control scheme of Sloan et al. [39], at the cost of a small strain increment. The initial void ratio was set to $e_0 = e^* + \Delta e_i$ with $e^* = 0.8$ at $p'_{y,i}$, so that soils with more structure started looser, as Eq. (1) requires. The integration was vectorised so that thousands of parameter sets could be advanced together. Poisson's ratio was fixed at $\nu = 0.25$.

Verification

With $\Delta e_i \to 0$ the model reduces to MCC, for which the critical state is known in closed form: $p'_{cs} = p'_0 \cdot 2^{-(1-\kappa^*/\lambda^*)}$ in undrained compression and $p'_{cs} = 3p'_0/(3 - M^*)$ in drained compression [21]. Figure 2 compares the numerical and closed-form results for three parameter sets. The

error decreased linearly with the strain increment (Fig. 2c), confirming first-order convergence. At the increment adopted for the sensitivity analysis, $\Delta\varepsilon_d = 0.0025\%$, the error was 0.12% in the undrained critical-state mean stress and below 0.05% in the drained volumetric strain.

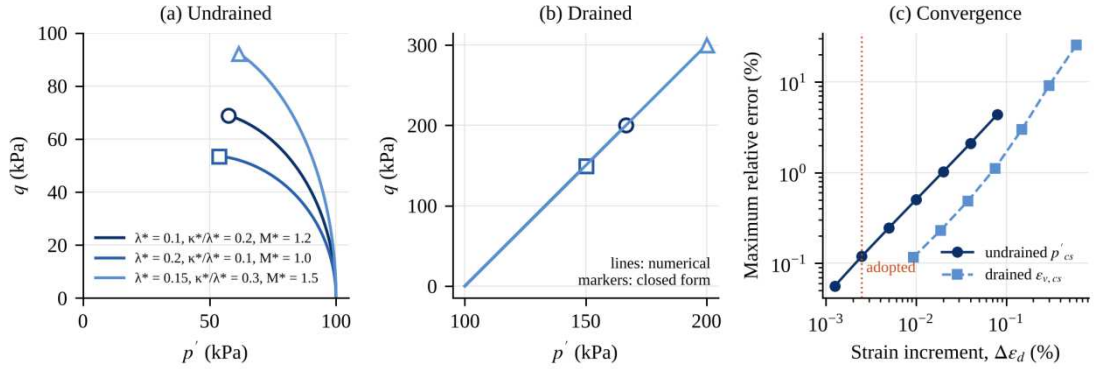


Fig. 2 Verification against closed-form Modified Cam Clay solutions. **a** Undrained and **b** drained effective stress paths for three parameter sets (lines: numerical; markers: closed form). **c** Convergence of the critical-state error with strain increment; the dotted line marks the increment adopted

Parameters, ranges and outputs

Seven parameters were treated as uncertain (Table 1). Two were reparameterised to make the inputs independent and physically admissible. The swelling index was sampled as the ratio κ^*/λ^*, and the flow-rule parameter as $\hat{\omega} = \omega\Delta e_i$, which lies between 0 and 1 by definition. Cohesion was normalised by $p'_{y,i}$. The ranges bracket values reported for lightly to moderately cemented clays [7, 8, 23, 24] and for the Isheri soils examined later. All distributions were uniform, reflecting the absence of prior information beyond the bounds.

Table 1 Parameters and sampling ranges

Parameter	Symbol	Lower	Upper	Isheri soils
Intrinsic compression index	λ^*	0.05	0.30	0.070–0.131

Parameter	Symbol	Lower	Upper	Isheri soils
Swelling-to-compression ratio	κ^*/λ^*	0.10	0.30	0.20 (assumed)
Critical state stress ratio	M^*	1.0	1.6	1.36–1.55
Additional void ratio at first yield	Δe_i	0.05	1.0	0.29–0.41
Destructuring index	b	0.1	5.0	0.5–5.0
Normalised flow-rule parameter	$\hat{\omega} = \omega\Delta e_i$	0	1.0	0.29–0.41
Normalised cohesion	$C/p'_{y,i}$	0	1.0	0.09–1.58

Seven outputs were examined (Table 2). Stresses were normalised by $p'_{y,i}$ so that the indices describe the shape of the response rather than its absolute scale.

Table 2 Model outputs examined in the sensitivity analysis

Stress path	Output	Definition	Physical meaning
Undrained	q_{max}	Peak deviator stress	Undrained strength
Undrained	ε_{50}	Deviatoric strain at 50% of q_{max}	Pre-failure stiffness
Undrained	ε_{95}	Deviatoric strain at 95% of q_{max}	Approach to failure
Undrained	Δu_f	Excess pore pressure at $\varepsilon_d = 20\%$	Pore pressure at failure
Drained	q_{15}	Deviator stress at $\varepsilon_d = 15\%$	Mobilised drained strength
Drained	$\varepsilon_{v,15}$	Volumetric strain at $\varepsilon_d = 15\%$	Volume change (compression)
Drained	ε_{50}	Deviatoric strain at 50% of q_{15}	Drained stiffness

Sobol' indices

For an output $Y = g(X_1, \ldots, X_k)$ with independent inputs, the first-order index S_i is the fraction of the output variance explained by X_i alone. The total-order index S_{Ti} also includes all interactions involving X_i [27, 30]:

$$S_i = \frac{V\left[E_{X_{\sim i}}(Y \mid X_i)\right]}{V(Y)}, \qquad S_{Ti} = \frac{E_{X_{\sim i}}\left[V_{X_i}(Y \mid X_{\sim i})\right]}{V(Y)} \qquad (10)$$

where $X_{\sim i}$ denotes all inputs except X_i. The indices were estimated with the Saltelli et al. [40] estimator for S_i and the Jansen [41] estimator for S_{Ti}, using two scrambled Sobol′ sequences

[42] of N = 2048 points and the k = 7 hybrid matrices [43], a total of N(k + 2) = 18 432 simulations for each stress path. Confidence intervals were obtained from 500 bootstrap resamples [44]. A parameter with $S_{Ti} < 0.05$ was regarded as non-influential for that output [27].

Identifiability

Sensitivity does not guarantee identifiability, because two influential parameters may compensate for each other [31]. Identifiability was therefore assessed by rejection sampling, in the spirit of generalised likelihood uncertainty estimation [32]. A reference parameter set close to Isheri soil S2 with moderate cementation (Table 3) was used to generate synthetic undrained and drained responses. Then 200 000 Latin hypercube samples [45] from the ranges of Table 1 were simulated, and a sample was accepted if all three outputs of a given test lay within ±10% of the reference values. This tolerance is comparable with the scatter between nominally identical triaxial specimens of cement-treated clay. A parameter was considered identifiable if the 5–95% range of the accepted values occupied a small fraction of its prior range.

Table 3 Reference parameter set used for the identifiability analysis

λ^*	κ^*/λ^*	M^*	Δe_i	b	$\hat{\omega}$	$C/p'_{y,i}$
0.103	0.2	1.52	0.408	0.6	0.408	0.4

The integrator and all post-processing were written in Python 3 using NumPy [46] for the vectorised integration. The scrambled Sobol′ sequences and Latin hypercube samples were generated with the quasi-Monte Carlo module of SciPy [47], the Sobol′ indices and their bootstrap confidence intervals were computed with the SALib library [48, 49], and the figures were prepared with Matplotlib [50].

Results and discussion

Local response

Figure 3 shows the local response about the reference set (with C = 0) as each parameter is varied across its range. In undrained compression (Fig. 3a–e), λ* changed the strain needed to mobilise strength several-fold but changed the peak by only 3%. Δe_i, b and $\hat{\omega}$ hardly affected either, whereas cohesion raised the peak almost linearly. In drained compression (Fig. 3f–j), the picture was reversed: Δe_i and b changed the volumetric strain at 15% shear by a factor of about three, $\hat{\omega}$ had a moderate effect and cohesion very little. Local results of this kind are informative but conditional on the reference point, and the global analysis below tests whether they hold across the parameter space.

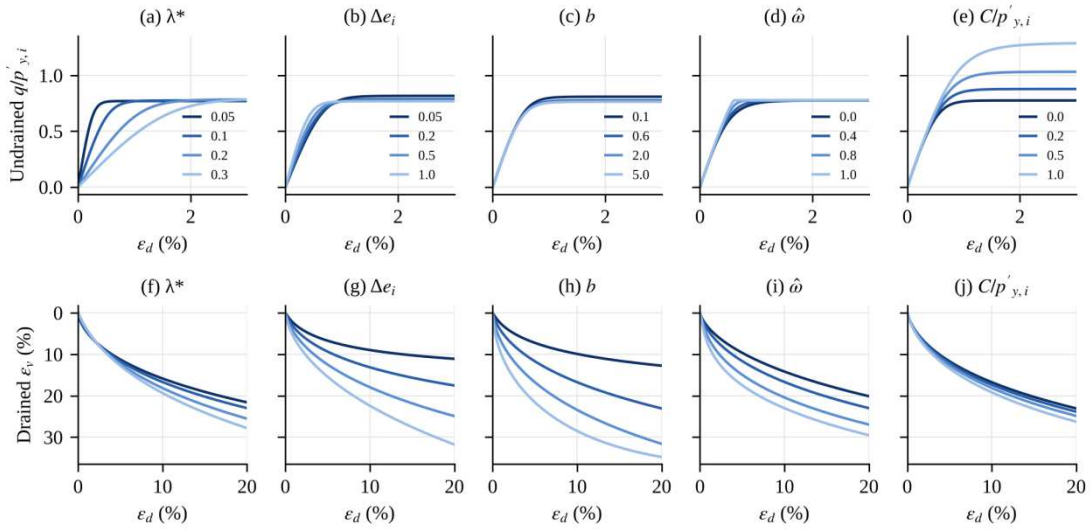


Fig. 3 One-at-a-time response about the reference set. **a–e** Undrained normalised deviator stress $q/p'_{y,i}$ against deviatoric strain ε_d. **f–j** Drained volumetric strain ε_v against ε_d

Global sensitivity indices

Figure 4 presents the total-order indices, with first-order indices in brackets. The bootstrap half-widths of the 95% confidence intervals did not exceed 0.055 for any index. The indices

also changed by less than 0.02 between N = 1024 and N = 2048 (Appendix B, Table 6), so the estimates are converged. The sums of first-order indices were 0.87–0.99 for the undrained outputs and 0.89–0.93 for the drained outputs, so interactions accounted for at most about 13% of the output variance. The model is therefore close to additive in its inputs over the ranges examined, which explains why the local trends of Fig. 3 were largely, though not entirely, preserved globally.

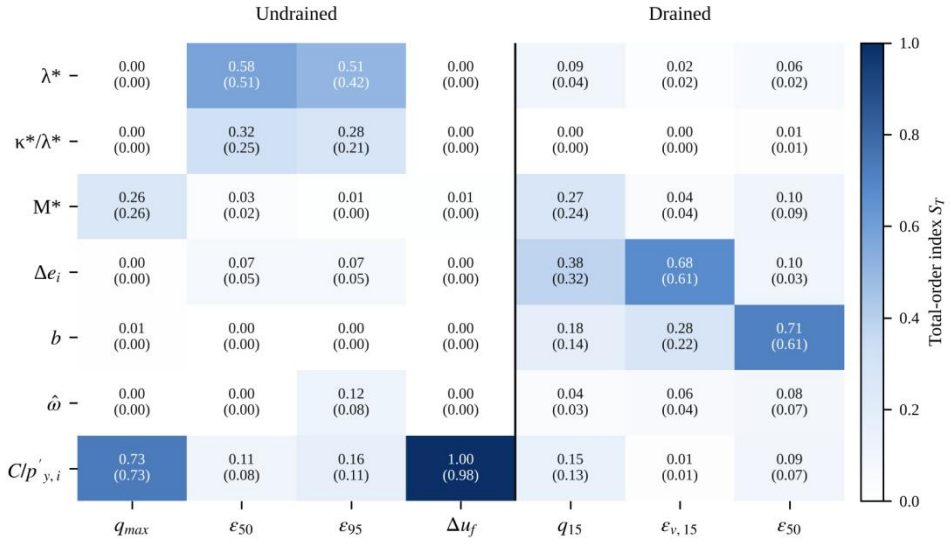


Fig. 4 Total-order Sobol′ indices S_T (first-order indices S_i in brackets) for the undrained and drained outputs

Three features stand out. First, the undrained peak strength depended on only two parameters, cohesion (S_T = 0.73) and M* (0.26). Every structural and compressibility parameter had $S_T \leq$ 0.01. The excess pore pressure at failure was governed by cohesion alone (S_T = 1.00). Second, the undrained stiffness measures ε_{50} and ε_{95} were controlled by λ* and κ*/λ* (combined $S_T \approx$ 0.8–0.9), that is, by the elastic modulus of Eq. (6) and the elastic–plastic partition it implies. The flow-rule parameter entered only ε_{95} (S_T = 0.12), as the stress state approached failure. Third, drained behaviour had an entirely different hierarchy. Δe_i dominated volumetric strain

(S_T = 0.68), b dominated drained stiffness (S_T = 0.71), and drained strength at 15% strain drew on Δe_i, M*, b and C together.

The practical consequence is that sensitivity is not a property of a parameter alone, but of a parameter, an output and a stress path together. A one-at-a-time study conducted under undrained loading would conclude, correctly for that path, that b is unimportant [26]. The same parameter is the most influential of all for drained stiffness. This mirrors the observation, made for natural structured clays, that destructuration governs volumetric response under drained loading far more than undrained strength [13–15].

Closed-form undrained strength

The insensitivity of undrained strength to the structural parameters has a simple explanation. At the critical state $\bar{\eta}$ = M*, and Eq. (3) gives $\bar{p}' = \bar{p}'_s/2$, so $q_{cs} = M^*\bar{p}'_{s,cs}/2$. In undrained shear, the yield surface can grow only through the plastic volumetric strain that balances elastic swelling. Equation (4) shows that this growth is resisted by the modulus A, which is at least $(\lambda^* - \kappa^*) + b\Delta e$ and becomes unbounded as $\bar{\eta} \rightarrow$ M*. When structure is significant, as measured by the structural ratio

$$\psi = \frac{b\,\Delta e_i}{\lambda^* - \kappa^*} \qquad (11)$$

the yield surface barely grows during undrained shear, so $\bar{p}'_{s,cs} \approx p'_{y,i} + C/M^*$, and (Appendix A)

$$q_{\max} \approx \frac{M^* p'_{y,i} + C}{2}, \qquad s_u \approx \frac{M^* p'_{y,i} + C}{4} \qquad (12)$$

In the opposite limit, $\psi \rightarrow 0$ with C = 0, the MCC result $q_{max} = M^* p'_{y,i} \cdot 2^{-(1-\kappa^*/\lambda^*)}$ is recovered, which exceeds Eq. (12) by a factor of $2^{\kappa^*/\lambda^*}$. Equation (12) is therefore a lower bound.

Figure 5 tests Eq. (12) against all 2048 parameter sets of the base sample. The ratio of simulated to predicted strength lay between 1.00 and 1.19, with a mean of 1.018. The prediction was within 5% for 92% of the sets, and within 3% for 96% of the sets with $\psi > 2$. Equation (12) also explains why each kilopascal of cohesion adds about half a kilopascal to the undrained peak, and why cohesion governs the pore pressure: the quantity C/M* simply shifts the stress path, so a larger part of the deviator stress is carried by bonding rather than by effective stress. For practice, Eq. (12) provides a quick, conservative check on any SCC calibration: if the simulated undrained strength of a structured cemented clay differs markedly from $(M^* p'_{y,i} + C)/2$, either ψ is small or the parameters are inconsistent.

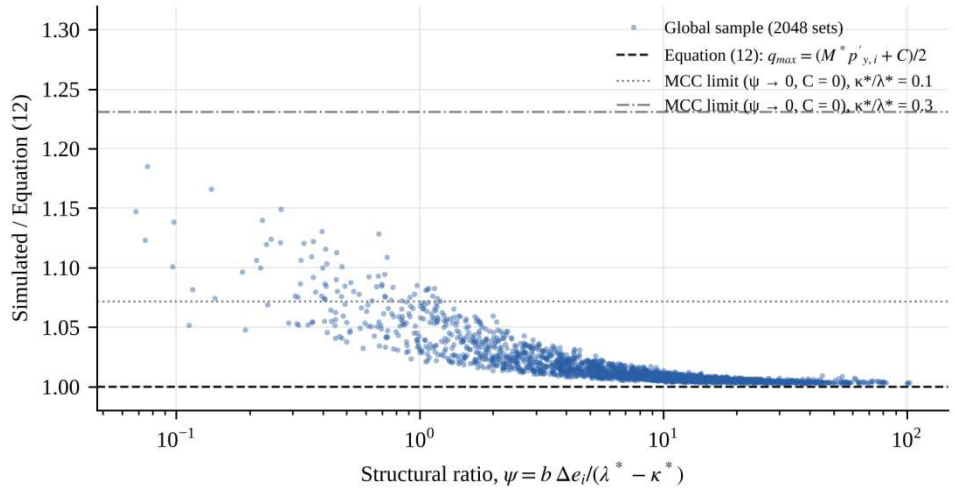


Fig. 5 Ratio of simulated undrained strength to Eq. (12) against the structural ratio ψ for the 2048 base-sample parameter sets; horizontal lines show the Modified Cam Clay limits for $\kappa^*/\lambda^* = 0.1$ and 0.3

Parameter identifiability

Of the 200 000 samples, 2278 reproduced the undrained reference response, 656 the drained response and 23 both. Figure 6a plots M* against C for the undrained acceptances. They fall along the line $M^* + C/p'_{y,i} \approx 1.92$ predicted by Eq. (12), with a correlation coefficient of

−0.81. Values of M* anywhere between 1.0 and 1.6 fit the undrained test equally well, provided cohesion compensates. A single undrained test therefore cannot separate frictional from cohesive strength, however well its curve is matched.

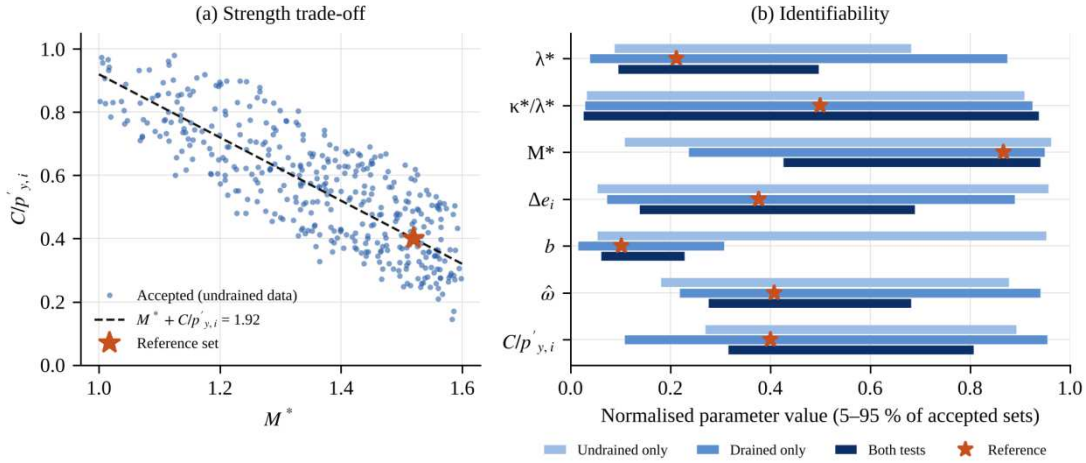


Fig. 6 Identifiability. **a** Trade-off between M* and C among parameter sets reproducing the undrained reference response. **b** Normalised 5–95% ranges of accepted parameters for undrained, drained and combined data; stars mark the reference set

Figure 6b summarises the 5–95% ranges of all accepted sets. With undrained data alone, every parameter retained at least 59% of its prior range. Drained data constrained b well (normalised width 0.29) but little else. Combining both tests narrowed λ*, Δe_i, $\hat{\omega}$ and C to roughly half their prior ranges and b to 0.17, but κ*/λ* remained unidentifiable (0.91). Even with both tests, M* and C remained strongly correlated (r = −0.93). These results are consistent with the indices of Fig. 4 and lead to a clear conclusion: SCC should not be calibrated by fitting all parameters simultaneously to triaxial stress–strain curves, a practice that is common when optimisation algorithms are applied to soil models [36, 37]. Without prior constraints, such fits can return parameter sets that reproduce the calibration tests but extrapolate poorly to other stress paths.

Staged calibration protocol

Table 4 turns the sensitivity and identifiability results into a calibration sequence in which each parameter is fixed from the measurement that isolates it, before any curve fitting. Compression tests on both the natural (or treated) and the reconstituted soil are needed for λ^*, Δe_i and b, consistent with the intrinsic-state framework [9, 19], and an unload–reload loop is needed for κ^*. M^* and C must be separated using tests at two or more effective confining pressures. Only ω, which had little influence on any output ($S_T \leq 0.12$), is reasonably left to a final adjustment of the drained curve or fixed at a default value.

Table 4 Staged calibration protocol for SCC with cohesion

Stage	Parameter(s)	Recommended test	Basis in this study
1	λ^*, e^*_{IC}	Isotropic or oedometer compression of reconstituted soil	Controls undrained stiffness (S_T = 0.51–0.58); not recoverable from triaxial fits
2	κ^*	Unload–reload loop in compression test	Not identifiable from triaxial curves (Fig. 6b)
3	$p'_{y,i}$, Δe_i, b	Compression of natural or treated soil compared with Stage 1	Dominate drained ε_v and stiffness (S_T up to 0.71)
4	M^*, C	Peak and critical states at two or more confining pressures	Trade off almost perfectly in a single test (Fig. 6a)
5	ω	Final adjustment to a drained curve, or default $\hat{\omega} \approx 0.5$	Weak influence ($S_T \leq 0.12$)

Application to cement-treated sandy clays

The protocol and Eq. (12) were applied to five sandy clays from Isheri, on the Lagos–Ogun boundary in Southwest Nigeria, treated with 0 and 9% ordinary Portland cement (OPC). Their parameters had been identified largely in the manner of Table 4, with M^* from end-of-test stress states and λ^* from the liquid limit. The exception was the swelling index: the slopes obtained from loading curves (0.12–0.21) exceeded λ^*, which is physically inadmissible, and $\kappa^* = 0.2\lambda^*$ was adopted instead. This is exactly the situation that the identifiability analysis

predicts when κ* is not measured directly. Table 5 lists the cohesion, structural ratio and simulated responses.

Table 5 Simulated response of five cement-treated Isheri soils ($p'_{y,i}$ = 100 kPa); errors are relative to the simulated strength

Soil	Cement content (%)	C (kPa)	ψ	q_{max} simulated (kPa)	q_{max} Eq. (12) (kPa)	Error (%)	Undrained ε_{50} (%)	Drained q_{15} (kPa)	Drained $\varepsilon_{v,15}$ (%)
S1	0	25	1.4	87.6	84.5	3.5	0.43	196	17.1
S1	9	158	1.4	159.7	151.0	5.4	0.80	317	20.3
S2	0	18	3.0	86.8	85.0	2.1	0.31	196	20.9
S2	9	70	3.0	113.5	111.0	2.2	0.41	245	22.5
S3	0	11	4.0	84.4	83.0	1.7	0.21	203	19.3
S3	9	19	4.0	88.5	87.0	1.7	0.22	211	19.6
S4	0	9	27.6	72.8	72.5	0.4	0.19	168	25.6
S4	9	22	27.6	79.4	79.0	0.5	0.20	191	25.6
S5	0	15	5.0	79.6	78.5	1.4	0.27	157	22.4
S5	9	24	5.0	84.2	83.0	1.4	0.29	164	22.8

Equation (12) reproduced the simulated undrained strengths to within 0.4–5.4%. The largest errors were for soil S1, which has the smallest structural ratio (ψ = 1.4) and, with 9% cement, a normalised cohesion ($C/p'_{y,i}$ = 1.58) above the upper bound of the sampled range. Both observations are consistent with Fig. 5, in which the scatter about Eq. (12) increases as ψ falls below about 2. The undrained strength gain from cement was large for S1 (+82%) and S2 (+31%) but small for the other three soils, in direct proportion to the measured gain in cohesion, as Eq. (12) requires. The drained response told a different story. Soil S4, whose destructuring index is ten times that of the others, had a drained ε_{50} of about 9%, against 3–5% for the rest, and the largest volumetric strain, almost regardless of cement content. For this soil, a design based on undrained strength alone would miss the property most likely to govern its long-term settlement.

Limitations

The analysis was restricted to triaxial compression from a normally consolidated, isotropic state at first virgin yield. Overconsolidated states [25], extension and cyclic loading may rank the parameters differently. The yield surface is isotropic, whereas natural and cement-treated clays generally show anisotropy that rotates and distorts it [18, 51, 52]; an anisotropic extension would add parameters whose identifiability should be examined in the same way. Cohesion was held constant, so post-peak softening due to debonding [16, 17] was not represented; including it would probably raise the influence of C on the strain measures. The inputs were treated as independent and uniform. In real soils, cement content raises C and Δe_i together, and correlated priors derived from test databases would sharpen the identifiability results. Finally, the identifiability analysis used synthetic data with a ±10% acceptance tolerance; real data with systematic errors may constrain the parameters less well.

Conclusions

A verified strain-driven integration of the Structured Cam Clay model with cohesion was used to carry out, to the authors' knowledge, the first variance-based sensitivity and identifiability analysis of the model under drained and undrained triaxial compression. The main conclusions are as follows.

1. Parameter influence depended strongly on stress path. Undrained peak strength was governed by cohesion ($S_T = 0.73$) and M* (0.26), and undrained stiffness by λ^* and κ^*/λ^*. Drained volume change and stiffness were governed by the structural parameters Δe_i (0.68) and b (0.71).

2. When structure is significant ($\psi = b\Delta e_i/(\lambda^* - \kappa^*)$ greater than about 2), the undrained strength of structured cemented clay sheared from first yield is well approximated by

$q_{max} \approx (M^* p'_{y,i} + C)/2$. This lower bound was within 5% of the full simulation for 92% of the sampled parameter sets.

3. M* and C traded off almost perfectly in a single undrained test, and κ* could not be identified from triaxial curves even when drained and undrained tests were combined.

4. The flow-rule parameter had little influence on any output examined ($S_T \leq 0.12$) and can be fixed at a default value without material loss of accuracy.

5. A staged calibration protocol based on compression tests, unload–reload loops and tests at two or more confining pressures was proposed. Applied to five cement-treated Isheri soils, it showed that the soil with the most brittle structure, although unremarkable in undrained strength, was the most compressible in drained shear.

Appendix A: Derivation of Eq. (12)

At the critical state $\bar{\eta} = M^*$, so $q = M^* \bar{p}'$. Substituting into Eq. (3) gives $\bar{p}' = \bar{p}'_s/2$, hence

$$q_{cs} = \frac{M^*}{2} \bar{p}'_{s,cs} \qquad \text{(A1)}$$

In undrained shear, $d\varepsilon_v^p = -d\varepsilon_v^e = -\kappa^* dp'/[(1+e)p']$, and Eq. (4) gives $dp'_s/p'_s = -(\kappa^*/A)\, dp'/p'$. Since $A \geq (\lambda^* - \kappa^*)(1 + \psi\, \Delta e/\Delta e_i)$ and p′ falls by at most a factor of about two between first yield and the critical state,

$$\ln \frac{p'_{s,cs}}{p'_{y,i}} \leq \frac{\kappa^*}{(\lambda^* - \kappa^*)(1+\psi)} \ln 2 \qquad \text{(A2)}$$

which vanishes as ψ becomes large. Then $\bar{p}'_{s,cs} \to p'_{y,i} + C/M^*$, and Eq. (A1) becomes Eq. (12). Because p'_s can only grow during loading, Eq. (12) is a lower bound. Equation (A2) is approximate, because Δe itself decays as p'_s grows. For ψ = 0 and C = 0, integration without the structural term gives the MCC result $p'_{cs} = p'_{y,i} \cdot 2^{-(1-\kappa^*/\lambda^*)}$.

Appendix B: Convergence of Sobol′ indices

Table 6 Total-order indices of four outputs for increasing base sample size N

Output	N	λ*	κ*/λ*	M*	Δe_i	b	$\hat{\omega}$	C
Undrained q_{max}	512	0.00	0.00	0.26	0.00	0.01	0.00	0.73
	1024	0.00	0.00	0.26	0.00	0.01	0.00	0.73
	2048	0.00	0.00	0.26	0.00	0.01	0.00	0.73
Undrained ε_{50}	512	0.56	0.32	0.03	0.07	0.00	0.00	0.11
	1024	0.58	0.32	0.03	0.07	0.00	0.00	0.11
	2048	0.58	0.32	0.03	0.07	0.00	0.00	0.11
Drained q_{15}	512	0.10	0.00	0.27	0.40	0.17	0.04	0.15
	1024	0.10	0.00	0.27	0.40	0.18	0.04	0.15
	2048	0.09	0.00	0.27	0.38	0.18	0.04	0.15
Drained $\varepsilon_{v,15}$	512	0.02	0.00	0.04	0.71	0.27	0.05	0.01
	1024	0.02	0.00	0.04	0.70	0.28	0.06	0.01
	2048	0.02	0.00	0.04	0.68	0.28	0.06	0.01

Nomenclature

Table 7 List of symbols

Symbol	Description
A	Plastic hardening modulus term, Eq. (4)
b	Destructuring index
C	Cohesion (kPa)
$D(\bar{\eta})$	Dilatancy function, Eq. (5)
e, e*	Void ratio of structured and reconstituted soil
e^*_{IC}	Void ratio of reconstituted soil on the isotropic compression line at p′ = 1 kPa
Δe, Δe_i	Additional void ratio; its value at first virgin yield
G, K	Elastic shear and bulk moduli (kPa)
M*	Critical state stress ratio
N, k	Base sample size; number of uncertain parameters
p′, $\bar{p}'$	Mean effective stress; shifted by cohesion, p′ + C/M* (kPa)
p'_s	Size of the structural yield surface (kPa)
$p'_{y,i}$	Mean effective stress at first virgin yield (kPa)
q	Deviator stress (kPa)
S_i, S_{Ti}	First-order and total-order Sobol′ indices

Symbol	Description
s_u	Undrained shear strength (kPa)
Δu_f	Excess pore pressure at ε_d = 20% (kPa)
ε_d, ε_v	Deviatoric and volumetric strain
ε_{50}, ε_{95}	Deviatoric strain at 50% and 95% of peak deviator stress
$\bar{\eta}$	Stress ratio $q/\bar{p}'$
κ^*, λ^*	Swelling and intrinsic compression indices
ν	Poisson's ratio
ψ	Structural ratio $b\Delta e_i/(\lambda^* - \kappa^*)$
ω, $\hat{\omega}$	Flow-rule parameter; normalised form $\omega\Delta e_i$
Λ	Plastic multiplier

Abbreviations

CI: Confidence interval; MCC: Modified Cam Clay; OPC: Ordinary Portland cement; SCC: Structured Cam Clay.

Declarations

Availability of data and materials

The integration code, sampling matrices and simulation outputs supporting the conclusions of this article are available from the corresponding author on reasonable request.

Competing interests

The authors declare that they have no competing interests.

Funding

This research received no specific grant from any funding agency in the public, commercial or not-for-profit sectors.

Authors' contributions

AAI conceived and designed the study, developed the methodology and software, performed the verification, formal analysis and investigation, curated the data, prepared the visualisations, and wrote the original draft. NK-O and SAA contributed to the interpretation of the results and to reviewing and editing the manuscript. All authors read and approved the final manuscript.

Acknowledgements

Not applicable.

References

1. Miura N, Horpibulsuk S, Nagaraj TS (2001) Engineering behavior of cement stabilized clay at high water content. Soils Found 41(5):33–45. https://doi.org/10.3208/sandf.41.5_33
2. Horpibulsuk S, Miura N, Bergado DT (2004) Undrained shear behavior of cement admixed clay at high water content. J Geotech Geoenviron Eng 130(10):1096–1105. https://doi.org/10.1061/(ASCE)1090-0241(2004)130:10(1096)
3. Lorenzo GA, Bergado DT (2004) Fundamental parameters of cement-admixed clay – new approach. J Geotech Geoenviron Eng 130(10):1042–1050. https://doi.org/10.1061/(ASCE)1090-0241(2004)130:10(1042)
4. Kamruzzaman AHM, Chew SH, Lee FH (2009) Structuration and destructuration behavior of cement-treated Singapore marine clay. J Geotech Geoenviron Eng 135(4):573–589. https://doi.org/10.1061/(ASCE)1090-0241(2009)135:4(573)
5. Horpibulsuk S, Miura N, Nagaraj TS (2003) Assessment of strength development in cement-admixed high water content clays with Abrams' law as a basis. Géotechnique 53(4):439–444. https://doi.org/10.1680/geot.2003.53.4.439
6. Horpibulsuk S, Rachan R, Chinkulkijniwat A, Raksachon Y, Suddeepong A (2010) Analysis of strength development in cement-stabilized silty clay from microstructural considerations. Constr Build Mater 24(10):2011–2021. https://doi.org/10.1016/j.conbuildmat.2010.03.011

7. Kasama K, Ochiai H, Yasufuku N (2000) On the stress-strain behaviour of lightly cemented clay based on an extended critical state concept. Soils Found 40(5):37–47. https://doi.org/10.3208/sandf.40.5_37
8. Lee K, Chan D, Lam K (2004) Constitutive model for cement treated clay in a critical state frame work. Soils Found 44(3):69–77. https://doi.org/10.3208/sandf.44.3_69
9. Burland JB (1990) On the compressibility and shear strength of natural clays. Géotechnique 40(3):329–378. https://doi.org/10.1680/geot.1990.40.3.329
10. Leroueil S, Vaughan PR (1990) The general and congruent effects of structure in natural soils and weak rocks. Géotechnique 40(3):467–488. https://doi.org/10.1680/geot.1990.40.3.467
11. Cotecchia F, Chandler RJ (2000) A general framework for the mechanical behaviour of clays. Géotechnique 50(4):431–447. https://doi.org/10.1680/geot.2000.50.4.431
12. Gens A, Nova R (1993) Conceptual bases for a constitutive model for bonded soils and weak rocks. In: Anagnostopoulos A, Schlosser F, Kalteziotis N, Frank R (eds) Geotechnical engineering of hard soils – soft rocks. Balkema, Rotterdam, pp 485–494
13. Rouainia M, Muir Wood D (2000) A kinematic hardening constitutive model for natural clays with loss of structure. Géotechnique 50(2):153–164. https://doi.org/10.1680/geot.2000.50.2.153
14. Kavvadas M, Amorosi A (2000) A constitutive model for structured soils. Géotechnique 50(3):263–273. https://doi.org/10.1680/geot.2000.50.3.263
15. Baudet B, Stallebrass S (2004) A constitutive model for structured clays. Géotechnique 54(4):269–278. https://doi.org/10.1680/geot.2004.54.4.269
16. Nguyen L, Fatahi B, Khabbaz H (2014) A constitutive model for cemented clays capturing cementation degradation. Int J Plast 56:1–18. https://doi.org/10.1016/j.ijplas.2014.01.007
17. Yamada S, Sakai T, Nakano M, Noda T (2022) Method to introduce the cementation effect into existing elastoplastic constitutive models for soils. J Geotech Geoenviron Eng 148(5). https://doi.org/10.1061/(ASCE)GT.1943-5606.0002727
18. Dejaloud H, Rezania M (2021) Adaptive anisotropic constitutive modeling of natural clays. Int J Numer Anal Methods Geomech 45(12):1756–1790. https://doi.org/10.1002/nag.3223
19. Liu MD, Carter JP (2002) A structured Cam Clay model. Can Geotech J 39(6):1313–1332. https://doi.org/10.1139/t02-069

20. Roscoe KH, Burland JB (1968) On the generalized stress–strain behaviour of wet clay. In: Heyman J, Leckie FA (eds) Engineering plasticity. Cambridge University Press, Cambridge, pp 535–609
21. Muir Wood D (1990) Soil behaviour and critical state soil mechanics. Cambridge University Press, Cambridge
22. Schofield AN, Wroth CP (1968) Critical state soil mechanics. McGraw-Hill, London
23. Horpibulsuk S, Liu MD, Liyanapathirana DS, Suebsuk J (2010) Behaviour of cemented clay simulated via the theoretical framework of the Structured Cam Clay model. Comput Geotech 37(1–2):1–9. https://doi.org/10.1016/j.compgeo.2009.06.007
24. Suebsuk J, Horpibulsuk S, Liu MD (2010) Modified Structured Cam Clay: a generalised critical state model for destructured, naturally structured and artificially structured clays. Comput Geotech 37(7–8):956–968. https://doi.org/10.1016/j.compgeo.2010.08.002
25. Suebsuk J, Horpibulsuk S, Liu MD (2011) A critical state model for overconsolidated structured clays. Comput Geotech 38(5):648–658. https://doi.org/10.1016/j.compgeo.2011.03.011
26. Igbeneghu AA, Osariyekemwen SA, Ikhide O (2026) Comparative sensitivity of Structured Cam Clay parameters in predicting the undrained behaviour of cement-treated soil. Int J Eng Res Technol 15(10):IJERTV15IS100060. https://doi.org/10.5281/zenodo.23186038
27. Saltelli A, Ratto M, Andres T, Campolongo F, Cariboni J, Gatelli D, Saisana M, Tarantola S (2008) Global sensitivity analysis: the primer. Wiley, Chichester
28. Iooss B, Lemaître P (2015) A review on global sensitivity analysis methods. In: Dellino G, Meloni C (eds) Uncertainty management in simulation-optimization of complex systems. Springer, Boston, pp 101–122. https://doi.org/10.1007/978-1-4899-7547-8_5
29. Sobol′ IM (1993) Sensitivity estimates for nonlinear mathematical models. Math Model Comput Exp 1(4):407–414
30. Sobol′ IM (2001) Global sensitivity indices for nonlinear mathematical models and their Monte Carlo estimates. Math Comput Simul 55(1–3):271–280. https://doi.org/10.1016/S0378-4754(00)00270-6

31. Brun R, Reichert P, Künsch HR (2001) Practical identifiability analysis of large environmental simulation models. Water Resour Res 37(4):1015–1030. https://doi.org/10.1029/2000WR900350
32. Beven K, Binley A (1992) The future of distributed models: model calibration and uncertainty prediction. Hydrol Process 6(3):279–298. https://doi.org/10.1002/hyp.3360060305
33. Ledesma A, Gens A, Alonso EE (1996) Estimation of parameters in geotechnical backanalysis – I. Maximum likelihood approach. Comput Geotech 18(1):1–27. https://doi.org/10.1016/0266-352X(95)00021-2
34. Calvello M, Finno RJ (2004) Selecting parameters to optimize in model calibration by inverse analysis. Comput Geotech 31(5):410–424. https://doi.org/10.1016/j.compgeo.2004.03.004
35. Finno RJ, Calvello M (2005) Supported excavations: observational method and inverse modeling. J Geotech Geoenviron Eng 131(7):826–836. https://doi.org/10.1061/(ASCE)1090-0241(2005)131:7(826)
36. Jin YF, Yin ZY, Shen SL, Hicher PY (2016) Selection of sand models and identification of parameters using an enhanced genetic algorithm. Int J Numer Anal Methods Geomech 40(8):1219–1240. https://doi.org/10.1002/nag.2487
37. Yin ZY, Jin YF, Shen SL, Hicher PY (2018) Optimization techniques for identifying soil parameters in geotechnical engineering: comparative study and enhancement. Int J Numer Anal Methods Geomech 42(1):70–94. https://doi.org/10.1002/nag.2714
38. Potts DM, Gens A (1985) A critical assessment of methods of correcting for drift from the yield surface in elasto-plastic finite element analysis. Int J Numer Anal Methods Geomech 9(2):149–159. https://doi.org/10.1002/nag.1610090204
39. Sloan SW, Abbo AJ, Sheng D (2001) Refined explicit integration of elastoplastic models with automatic error control. Eng Comput 18(1/2):121–154. https://doi.org/10.1108/02644400110365842
40. Saltelli A, Annoni P, Azzini I, Campolongo F, Ratto M, Tarantola S (2010) Variance based sensitivity analysis of model output. Design and estimator for the total sensitivity index. Comput Phys Commun 181(2):259–270. https://doi.org/10.1016/j.cpc.2009.09.018
41. Jansen MJW (1999) Analysis of variance designs for model output. Comput Phys Commun 117(1–2):35–43. https://doi.org/10.1016/S0010-4655(98)00154-4

42. Owen AB (1998) Scrambling Sobol′ and Niederreiter–Xing points. J Complex 14(4):466–489. https://doi.org/10.1006/jcom.1998.0487
43. Saltelli A (2002) Making best use of model evaluations to compute sensitivity indices. Comput Phys Commun 145(2):280–297. https://doi.org/10.1016/S0010-4655(02)00280-1
44. Efron B, Tibshirani RJ (1993) An introduction to the bootstrap. Chapman & Hall, New York
45. McKay MD, Beckman RJ, Conover WJ (1979) A comparison of three methods for selecting values of input variables in the analysis of output from a computer code. Technometrics 21(2):239–245. https://doi.org/10.2307/1268522
46. Harris CR, Millman KJ, van der Walt SJ, Gommers R, Virtanen P, Cournapeau D et al (2020) Array programming with NumPy. Nature 585(7825):357–362. https://doi.org/10.1038/s41586-020-2649-2
47. Virtanen P, Gommers R, Oliphant TE, Haberland M, Reddy T, Cournapeau D et al (2020) SciPy 1.0: fundamental algorithms for scientific computing in Python. Nat Methods 17(3):261–272. https://doi.org/10.1038/s41592-019-0686-2
48. Herman J, Usher W (2017) SALib: an open-source Python library for sensitivity analysis. J Open Source Softw 2(9):97. https://doi.org/10.21105/joss.00097
49. Iwanaga T, Usher W, Herman J (2022) Toward SALib 2.0: advancing the accessibility and interpretability of global sensitivity analyses. Socio-Environ Syst Model 4:18155. https://doi.org/10.18174/sesmo.18155
50. Hunter JD (2007) Matplotlib: a 2D graphics environment. Comput Sci Eng 9(3):90–95. https://doi.org/10.1109/MCSE.2007.55
51. Wheeler SJ, Näätänen A, Karstunen M, Lojander M (2003) An anisotropic elastoplastic model for soft clays. Can Geotech J 40(2):403–418. https://doi.org/10.1139/t02-119
52. Karstunen M, Krenn H, Wheeler SJ, Koskinen M, Zentar R (2005) Effect of anisotropy and destructuration on the behavior of Murro test embankment. Int J Geomech 5(2):87–97. https://doi.org/10.1061/(ASCE)1532-3641(2005)5:2(87)